

Nanoscale

Accepted Manuscript

This article can be cited before page numbers have been issued, to do this please use: S. H. Park, G. M. Seo, J. W. Kim, Y. H. Lee, G. Lee, H. J. Lee and B. D. Kong, *Nanoscale*, 2025, DOI: 10.1039/D5NR04252F.



This is an Accepted Manuscript, which has been through the Royal Society of Chemistry peer review process and has been accepted for publication.

Accepted Manuscripts are published online shortly after acceptance, before technical editing, formatting and proof reading. Using this free service, authors can make their results available to the community, in citable form, before we publish the edited article. We will replace this Accepted Manuscript with the edited and formatted Advance Article as soon as it is available.

You can find more information about Accepted Manuscripts in the [Information for Authors](#).

Please note that technical editing may introduce minor changes to the text and/or graphics, which may alter content. The journal's standard [Terms & Conditions](#) and the [Ethical guidelines](#) still apply. In no event shall the Royal Society of Chemistry be held responsible for any errors or omissions in this Accepted Manuscript or any consequences arising from the use of any information it contains.

ARTICLE

Scalable Synthesis of Spatially Confined Ge Quantum Dots with Tunable Quantum Confinement

Su Hyun Park^a, Gyeong Min Seo^a, Jeong Wook Kim^a, Yun Ho Lee^a, Gyubin Lee^a, Hong Jae Lee^a, and Byoung Don Kong^{*a}

Received 00th January 20xx,
Accepted 00th January 20xx

DOI: 10.1039/x0xx00000x

We report a scalable, thermodynamically guided method for synthesizing germanium quantum dots embedded in a silicon oxide matrix with nanometer-scale precision. By engineering the oxidation and annealing conditions of silicon–germanium alloy layers, we achieve spatially confined, crystalline germanium quantum dots as small as 9.2 nanometers with tunneling oxide thicknesses down to 3.2 nanometers—suitable for room-temperature quantum confinement. Molecular dynamics simulations across a range of germanium compositions predict the agglomeration behaviour and size evolution of the quantum dots, while an analytical model enables predictive tuning of quantum dot dimensions and oxide thickness based on initial alloy composition. Experimental validation using scanning transmission electron microscopy, X-ray diffraction, and photoluminescence confirms crystallinity and size-dependent optical emission in the visible range. In contrast to earlier nanocrystal memory systems that relied on randomly distributed germanium precipitates embedded deep in thick oxide, our method enables precise formation of shallow, single-layer quantum dots with controlled geometry. These findings establish a robust platform for room-temperature quantum dot electronics, combining tunable confinement and compatibility with integrated circuit architectures.

1 Introduction

Semiconductor quantum dots (QDs), owing to their discrete energy levels and tunable quantum properties, underpin many of today's most promising advances in quantum materials and nanodevices.¹ Since the pioneering work of Louis Brus—who first demonstrated that the electronic structure of nanocrystals could be tailored by size²—colloidal and solid-state QDs have enabled a wide spectrum of technologies, from light-emitting devices to memory and sensing platforms. In contrast to potential-well-based systems that often require cryogenic operation, nanocrystal-based QDs offer robust quantum confinement even at room temperature, making them particularly attractive for scalable quantum electronics.^{3–8}

In solid-state systems, Ge nanocrystals spontaneously form in oxide matrices such as SiGeO during thermal processing. This phenomenon was originally discovered not in the pursuit of quantum control, but in the context of CMOS device fabrication, where Ge aggregation during SiGe oxidation complicated the formation of uniform gate dielectrics.^{9,10} Later, researchers repurposed this self-assembly behaviour for nonvolatile memory,^{11–14} emphasizing charge retention over control of size, position, or interface proximity. These early systems featured randomly distributed Ge precipitates, often embedded deep

within thick oxide layers, and lacked the confinement precision required for fast, low-voltage quantum operations.^{15–18}

Formation of Ge nanostructures through oxidation of SiGe alloys has been previously reported.^{19–21} In these earlier studies, polycrystalline SiGe layers embedded between oxides were oxidized, and Ge nanocrystals were formed within the oxide matrix during annealing steps. In contrast, our approach is designed to generate a single, spatially uniform layer of Ge QDs from a single SiGe layer directly on the Si substrate. The low temperature oxidation step is first used to convert the SiGe film into a homogeneous SiGeO layer while preserving a high-quality interface between SiGe and oxide interface. Subsequent high temperature annealing then drives the self-limited condensation of Ge atoms into uniformly sized QDs. While both Si and Ge are oxidized at low temperatures, elevated annealing temperatures promote dissociation of Ge–O bonds, which are considerably less thermodynamically stable than Si–O bonds, thereby facilitating the precipitation of elemental Ge.^{16,22,23}

Here, we advance this concept by demonstrating a deterministic, self-assembly-based strategy for producing spatially confined, crystalline Ge QDs within a SiO_x matrix, positioned within 3.2 nm of the semiconductor interface. By carefully engineering the oxidation and double-step annealing of SiGe alloy layers, sub-10 nm Ge QDs are synthesized in a single plane, enabling tunable quantum confinement. The synthesis pathway is guided by molecular dynamics (MD) simulations and analytical modelling, allowing predictive design of QD size and tunnelling oxide thickness from initial

^a Department of Electrical Engineering, Pohang University of Science and Technology (POSTECH), Pohang 37673, Korea. E-Mail: bdkong@postech.ac.kr



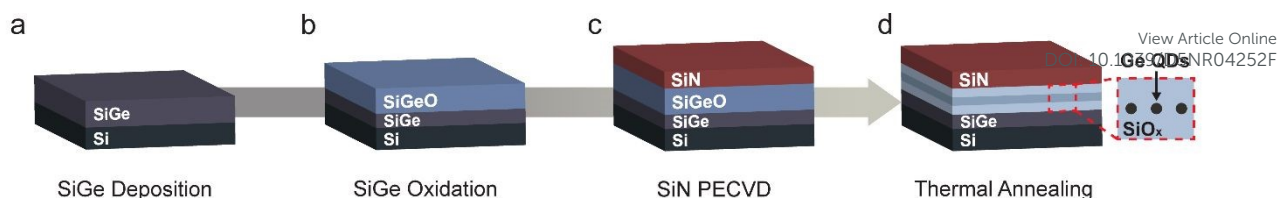


Fig. 1 (a-d) Schematic overview of the Ge QDs synthesis process. This process was followed in the experiments.

composition. Structural and photoluminescence characterization confirm quantum confinement effects at room temperature. The proposed synthesis method offers a practical and scalable approach for synthesizing Ge nanocrystal quantum dots (NCQDs) compatible with conventional Si-based technology. This work not only advances the understanding of selective oxidation and self-assembly mechanisms in the Si–Ge–O system but also provides a versatile platform for the fabrication of next-generation QD devices with broad applications in optoelectronics, memory, and sensing technologies.

2 Results and discussion

2.1 Ge quantum dots formation within oxide

The formation of Ge NCQDs was achieved by controlling the oxidation-driven transformation of the SiGe layer and subsequent thermal annealing. At oxidation temperatures below 600 °C, the activation energy for germanium diffusion exceeds the available thermal energy, leading to the formation of a homogeneous SiGeO alloy as both silicon and germanium are oxidized. Upon subsequent annealing at temperatures above 600 °C, the mobility of germanium atoms increases, enabling their diffusion and agglomeration. Due to the large thermodynamic stability difference between silicon dioxide and germanium dioxide as described by the Gibbs triangle of the Si–Ge–O system,^{24,25} elemental germanium becomes the energetically preferred phase, leading to the precipitation of crystalline nanodots.

The initial oxidation process differs from conventional thermal oxidation of silicon wafers; it employs a very low oxygen flow to form a precisely controlled nanometer-scale SiGeO alloy. As illustrated in Fig. 1, the process begins with the deposition of a $\text{Si}_x\text{Ge}_{1-x}$ film by molecular beam epitaxy (MBE) or ultra-high vacuum chemical vapor deposition (UHV-CVD), ensuring compatibility with standard silicon processing. Thermal oxidation was performed at 550–600 °C in a tube furnace under near-atmospheric pressure (770 Torr) with pure O_2 gas supplied at 20 sccm. In this low temperature regime, the diffusivities of Si and Ge decrease more sharply than the oxidation rate, allowing both elements to oxidize and form a homogeneous amorphous SiGeO alloy layer. By adjusting the oxidation duration, the thickness and composition of this intermediate layer can be precisely controlled.

To suppress further oxygen ingress during subsequent annealing, which may increase the thickness, a SiN capping layer

was deposited by plasma-enhanced chemical vapor deposition (PECVD). Actually, any dense material that can block the oxygen passage would serve for this, and indeed, for certain samples prepared for X-ray diffraction (XRD), a TiN layer was first deposited via atomic layer deposition (ALD), followed by the same SiN capping.

Post-oxidation, Ge NCQDs were formed through rapid thermal annealing (RTA) in nitrogen. Before annealing, the chamber was evacuated to $\sim 1 \times 10^{-3}$ Torr and then backfilled with N_2 to $\sim 1 \times 10^{-1}$ Torr. Two RTA strategies were employed: (1) a single-step annealing at 800 °C and (2) a double-step annealing consisting of an initial high-temperature pulse at 1000 °C followed by a lower-temperature step at 700–800 °C. According to the previous studies,¹⁵ the reduction of GeO_x is more promoted at higher temperature annealing, enabling the initial formation of Ge nanoparticles. As GeO_x defects are reduced during the first annealing at 1000 °C, the subsequent growth of Ge QDs occurs with improved size uniformity and spatial distribution within the oxide matrix. Further, vacuum conditions and pure N_2 ambient prevented reoxidation of Ge, facilitating phase-pure NCQD growth.

A critical feature of this method is the ability to control the vertical position of the Ge QDs and the surrounding oxide thickness by adjusting the thickness and composition of the SiGeO alloy. In our process, the SiGe layer is directly oxidized at low temperature, deliberately forming a homogeneous SiGeO alloy. After depositing a SiN capping layer, high temperature annealing drives Ge extraction from the SiGeO alloy. Importantly, this approach obviates the need for a separate

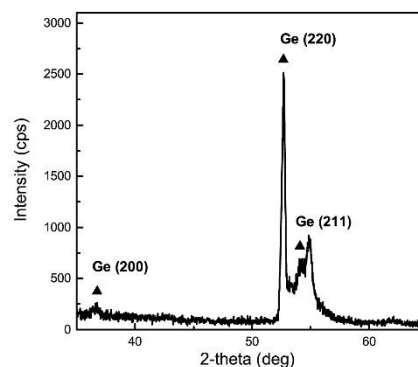
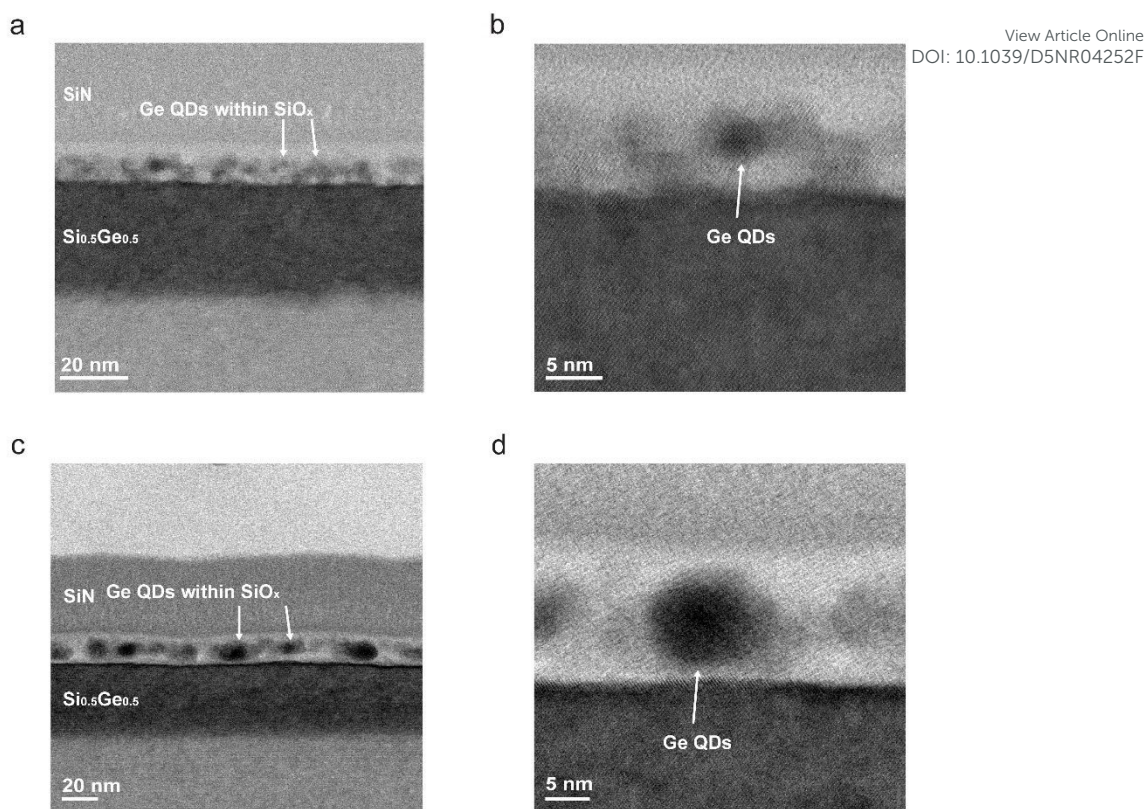


Fig. 2 XRD pattern of Ge QDs with single-step annealing process.





View Article Online
DOI: 10.1039/D5NR04252F

Fig. 3 Bright field STEM images of Ge NCQDs embedded in oxide after (a, b) single-step annealing and (c, d) double-step annealing.

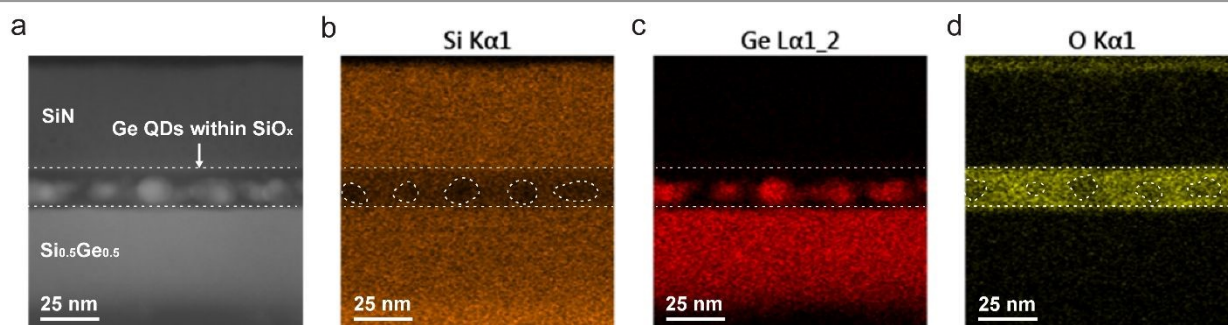


Fig. 4 EDS maps of the sample after double-step annealing. (a) Dark field STEM image. (b-d) Elemental distribution maps of Si, Ge and O corresponding to the STEM image.

tunnelling oxide growth step; an ultrathin tunnelling oxide forms spontaneously as the remaining SiGeO is converted to SiO₂ during the annealing process.

Controlling the oxidation time and the initial SiGe composition enables deterministic control over the final QD size and oxide thickness, as it dictates the absolute amount of available germanium for aggregation. Moreover, compared to ion implantation methods, which typically introduce germanium at concentrations below 10¹⁹ cm⁻³, this SiGe oxidation strategy offers much higher atomic densities (up to 10²² cm⁻³) and superior control over depth and spatial confinement. Achieving nanometer-scale vertical accuracy using ion implantation remains highly challenging, while our method enables intrinsic alignment near the channel region with sub-5 nm oxide encapsulation.

The formation of Ge NCQDs and their crystallinity were confirmed through structural and optical characterization. Cross-sectional scanning transmission electron microscopy (STEM) and X-ray diffraction (XRD) measurements. The STEM imaging of single-step annealed samples (800 °C, 30 minutes) revealed Ge NCQDs with rather large spatial distribution. The average diameter turned out to be 3.7 nm, and the total oxide thickness was ~12.0 nm (Fig. 3(b)). XRD results (Fig. 2) confirmed crystallinity with Bragg peaks corresponding to Ge(220) planes. The Ge(220) peak exhibited a full width at half maximum (FWHM) of 0.279°, further validating nanocrystal formation. Weak peaks at Ge(200) and (211) were also observed, which can be attributed to truncation effects and structural disorders arising from the nanoscale QD size.^{26,27}

The double-step annealing process appears more suitable to achieve improved spatial confinement for the controlled



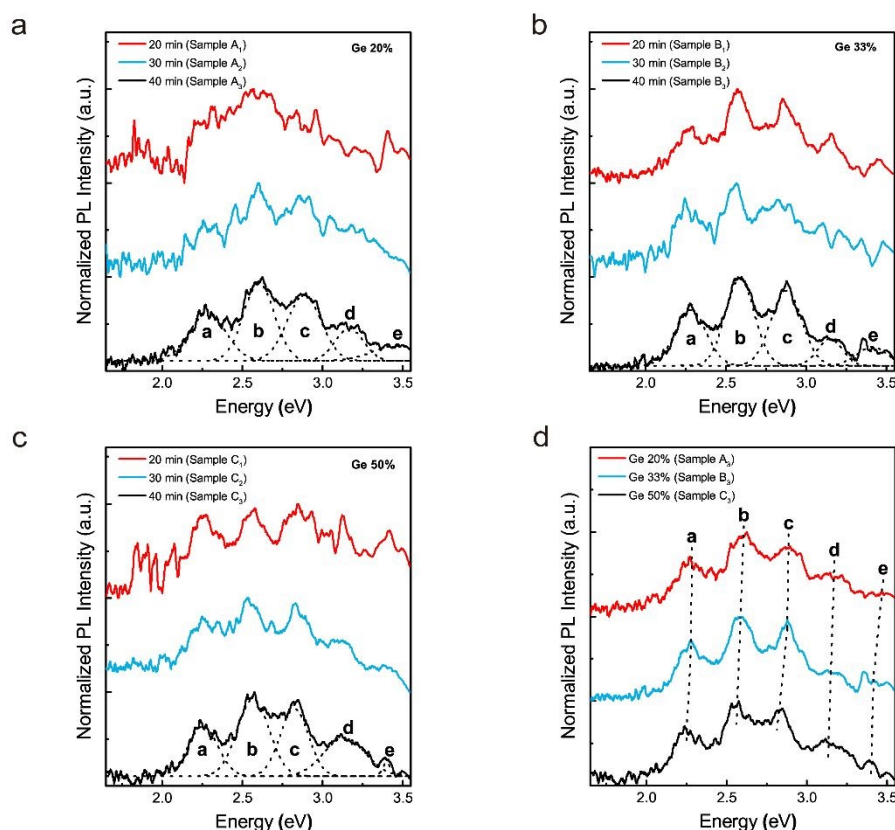


Fig. 5 (a–c) Normalized PL spectra of 9 samples at 300 nm (4.13 eV) excitation energy. The Ge concentrations in the $\text{Si}_{1-x}\text{Ge}_x$ layers used for Ge QDs formation vary by 20%, 33%, and 50%, corresponding to samples A_{1-3} , samples B_{1-3} , and samples C_{1-3} . In each sample group (A, B, and C), the Ge QDs growth times were controlled in 10-minute intervals. The sample numbers 1–3 correspond to growth times of 20, 30, and 40 minutes, respectively. Deconvolution analysis of the PL spectra at samples of 40 minutes was performed, with the resulting PL peaks marked as a, b, c, d, and e. (d) Normalized PL spectra of sample A_3 , sample B_3 , and sample C_3 . The Ge QDs growth time was 40 minutes. Dotted black lines indicate the shifts of each PL peak.

formation of QD arrays. For the double-step annealing process, the samples were first annealed at 1000 °C for 5 minutes, followed by a second step at 700 °C for 1 minute. This strategy leverages the enhanced mobility and reduction of GeO_x at high temperature to seed NCQD formation, while the second step stabilizes the growth and improves uniformity. As shown in Fig. 3(d), this method yielded a single row of Ge NCQDs embedded in a 17.8 nm-thick oxide layer, with QD diameters of ~9.2 nm and tunnelling oxide thickness as low as 3.2 nm. From the energy-dispersive spectroscopy (EDS) mapping in Fig. 4, nicely formed single layer of QDs with even spatial distribution can be clearly identified. The QDs are distinctly represented by red colour, with corresponding vacancies observed in the elemental

maps of other atoms.

The temperature design, such as the low temperature Si-Ge-O matrix formation and successive annealing appeared to be critical. The temperature-dependent oxidation behaviour of SiGe/Si layers was experimentally investigated at two different temperatures (600 °C and 850 °C) in near-atmospheric conditions, as detailed in the Supporting Information. At 850 °C, preferential oxidation of Si leads to Ge accumulation and the formation of a Ge-rich layer (GRL) near the SiO_2/SiGe interface (S.I. Fig. 3). In contrast, at 600 °C both Si and Ge oxidize, supporting SiGeO alloy formation. These observations align with prior thermodynamic studies and confirm the dual role of low temperature oxidation and high temperature annealing in producing confined crystalline Ge NCQDs. Consequently, the temperature-dependent behaviour of the Si-Ge-O system directly enabled the formation of a single row of Ge NCQDs through the double-step annealing process.

2.2 Optical evidence of quantum confinement

Optical properties were evaluated through photoluminescence (PL) spectroscopy, revealing discrete visible-light emission consistent with quantum confinement.²⁸ A total of nine samples were prepared from three types of $\text{Si}_{1-x}\text{Ge}_x/\text{Si}$ layers with different Ge contents ($x = 0.20, 0.33$, and 0.50). For each

Table 1 The positions of the PL peaks and FWHM properties for samples A_3 , B_3 , and C_3 with Ge QDs growth time of 40 minutes.

	Sample A_3		Sample B_3		Sample C_3	
	Peak (eV)	FWHM (eV)	Peak (eV)	FWHM (eV)	Peak (eV)	FWHM (eV)
a	2.283 ± 0.0015	0.271	2.281 ± 0.0008	0.226	2.255 ± 0.0011	0.216
B	2.604 ± 0.0015	0.227	2.588 ± 0.0007	0.212	2.568 ± 0.0014	0.234
c	2.885 ± 0.0016	0.251	2.877 ± 0.0009	0.224	2.824 ± 0.0015	0.207
d	3.167 ± 0.0045	0.207	3.149 ± 0.0025	0.179	3.138 ± 0.0027	0.304
e	3.466 ± 0.0137	0.361	3.412 ± 0.0038	0.222	3.400 ± 0.0021	0.059



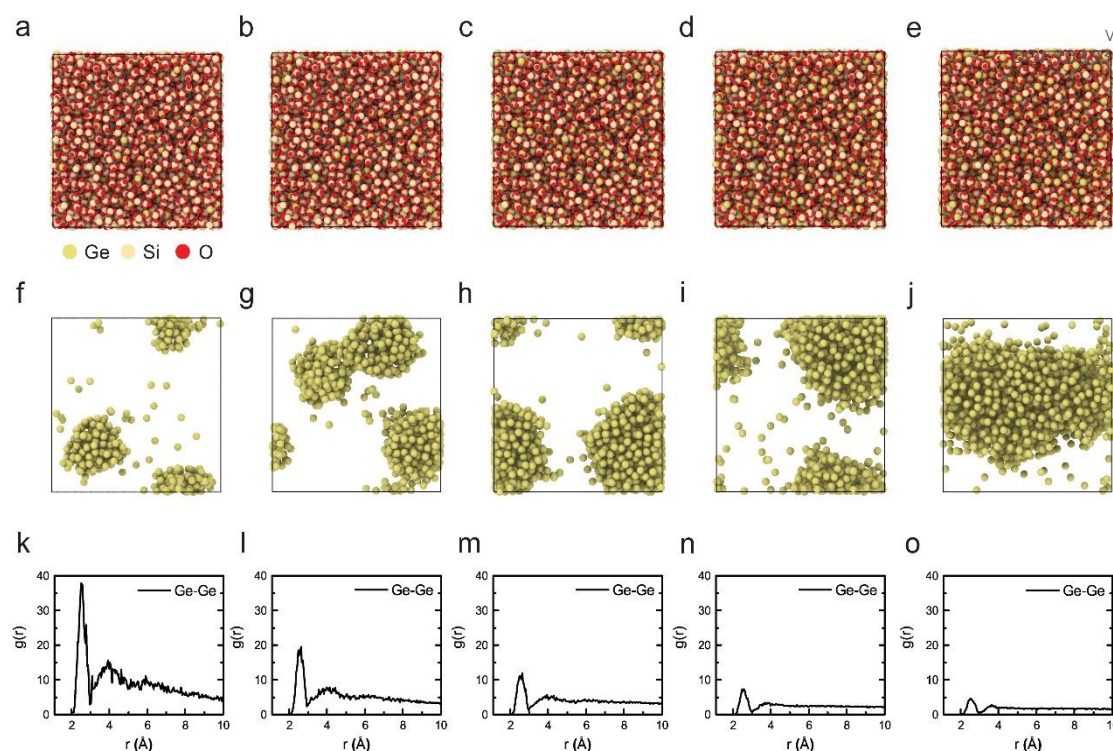


Fig. 6 Schematic illustrations for the Ge nanoparticle formation during the annealing process at 3000 K: (a-f) Initial structures and (g-j) final structure after 100 ns of the $\text{Si}_{0.9}\text{Ge}_{0.1}\text{O}_2$, $\text{Si}_{0.8}\text{Ge}_{0.2}\text{O}_2$, $\text{Si}_{0.7}\text{Ge}_{0.3}\text{O}_2$, $\text{Si}_{0.6}\text{Ge}_{0.4}\text{O}_2$, and $\text{Si}_{0.5}\text{Ge}_{0.5}\text{O}_2$ alloy. (k-j) PRDF graphs of Ge-Ge bonds investigated from the simulation results of the $\text{Si}_{0.9}\text{Ge}_{0.1}\text{O}_2$, $\text{Si}_{0.8}\text{Ge}_{0.2}\text{O}_2$, $\text{Si}_{0.7}\text{Ge}_{0.3}\text{O}_2$, $\text{Si}_{0.6}\text{Ge}_{0.4}\text{O}_2$, and $\text{Si}_{0.5}\text{Ge}_{0.5}\text{O}_2$ alloy.

composition, annealing durations of 20, 30, and 40 minutes were applied under 800 °C single-step RTA, yielding samples labelled A_{1-3} ($x = 0.20$), B_{1-3} ($x = 0.33$), and C_{1-3} ($x = 0.50$). PL spectra were measured at room temperature under laser excitation ranging from 300 to 650 nm. Among these, distinct emission peaks were most clearly observed under 300 nm excitation. As shown in Fig. 5(a–c) and summarized in Table 1, the PL emission exhibited strong dependence on both annealing time and Ge content. With increased annealing duration, five distinct peaks (labelled a–e) became progressively sharper and more separated, indicating improved NCQD size uniformity and enhanced thermodynamic stability. The highest intensity peak (b), observed in the C_3 sample ($x = 0.50$, 40 minutes), was centered at 2.568 eV with a FWHM of 0.234 eV. From the Brus equation,^{29,30} this corresponds to QDs radius of ~ 2.6 nm and a size variation of $\Delta R \sim 0.1$ nm, where R is the radius of QDs. ΔR can be considered as a size disorder in the system. These values exhibited excellent agreement with the average QD size of 5.2 nm observed in the STEM image of sample C_3 (S. I. Fig. 4(c)). While there were possibilities of the peaks originating from the optical resonance such as Fabry-Perot resonance due to the SiN_x capping layer, we excluded this possibility due to two reasons. Firstly, the resonance peak period differed from the value estimated from the SiN_x thickness, and secondly, the peak did not appear in other longer-wavelength regions, while there must have been some signature if it were a purely optical phenomenon. Considering the beam spot size of at least a few mm^2 in the PL measurement, this indicates the reasonable uniformity in QD sizes.

It is worth noting that even QDs of the same nominal size may differ structurally. For example, small aggregates of Au or Pt atoms can exhibit confinement-like effects without crystallinity. However, such non-crystalline clusters would not behave as semiconductor QDs: their discretized levels would be much smaller, requiring much smaller sizes to account for the observed PL range. In contrast, the agreement of our PL spectra with Brus formula, which assumes semiconductor effective masses derived from a periodic lattice, indicates that the Ge QDs here are at least partially crystalline. With respect to defects, only states within the band gap can contribute to PL, while states inside the bands are filled and inactive. The discrete energy levels we observed were much larger than typical defect-related energies, and no sub-gap peaks were detected, making it unlikely that intrinsic defect states are involved. One might also consider defect states in the Si or SiGe substrates; however, since both are indirect band gap materials and the observed PL emission is above 2 eV, it is unlikely that substrate-related defects contribute to the measured spectra.

A clear redshift in PL emission was observed with increasing Ge content—from $\text{Si}_{0.8}\text{Ge}_{0.2}$ to $\text{Si}_{0.5}\text{Ge}_{0.5}$ —consistent with quantum confinement behaviour (Fig. 5(d)). As the Ge supply in the Si–Ge–O matrices increases, the QD size increases, and the effective bandgap narrows, leading to lower-energy emission.³¹ Based on the PL peak positions presented in Table 1, the estimated QD diameters ranged from ~ 4 nm to ~ 6 nm across all sample sets. The emission wavelengths, spanning 358–550 nm,



demonstrate tunability within the visible spectrum through control of Ge content and annealing time.

These results underscore the role of annealing in achieving size-controlled QD formation. While 30 minutes of annealing was sufficient to produce crystalline Ge QDs, extending to 40 minutes yielded narrower and more reproducible PL peaks, indicating better size distribution and thermal stabilization. Collectively, the structural and optical data confirm that the Ge NCQDs exhibit pronounced quantum confinement effects and tunable optical properties at room temperature, positioning them as promising building blocks for integrated optoelectronic and quantum devices.

2.3 Modelling and predictive control of quantum dot size and distribution

To understand and predict the formation of Ge NCQDs within a SiO_x matrix, MD simulations using the Large-scale Atomic/Molecular Massively Parallel Simulator (LAMMPS) were conducted.³² The MD study provides cost-effective versatility that can supplement the experiments to obtain enough data to postulate a predictive QD formation modelling. A Tersoff potential was employed to model the Si–Ge–O ternary system (details provided in the Supporting Information). The simulations began with a base amorphous SiO_2 structure containing 4096 Si atoms and 8192 O atoms. Ge atoms were introduced by substituting Si atoms at various concentrations, yielding five alloy models with Ge contents of 10%, 20%, 30%, 40%, and 50%. Each simulation cell measured $5.70 \times 5.70 \times 5.70$ nm with periodic boundary conditions in all directions.

The samples were thermally annealed at 3000 K using an isothermal-isobaric (NPT) ensemble, a temperature below the melting point of Ge.³³ Although this temperature exceeds

realistic processing conditions, such elevated values are commonly used in MD simulations to accelerate atomic diffusion within computationally tractable timescales. Temperature and pressure were controlled via a Nose–Hoover thermostat and barostat with damping constants of 100 and 1000, respectively, and a 1 fs timestep was used throughout.

After 100 ns of simulated annealing, the formation of nearly spherical Ge clusters in samples was observed with up to 30% Ge content (Fig. 6(f–h)). In the 30% Ge sample, a single Ge NCQD was clearly resolved. For samples with 40% and 50% Ge (Fig. 6(i–j)), partial agglomeration occurred, but additional annealing would be required to achieve full spherical confinement. As shown in Fig. 6(k–o), partial radial distribution functions (PRDFs) were calculated to assess the atomic structure. First-neighbour Ge–Ge correlation peaks were found at 2.53 Å (10% Ge), 2.63 Å (20%, 30%), 2.48 Å (40%), and 2.53 Å (50%), with a lack of well-defined second or third peaks, suggesting that the Ge NCQDs were predominantly amorphous under the simulated conditions. This is consistent with the limited timescales of MD simulations, which constrain the development of long-range crystalline order. The average radii of Ge NCQDs were estimated as 0.68 nm, 0.89 nm, and 1.83 nm for the 10%, 20%, and 30% Ge models, respectively. These results indicate a direct scaling relationship between Ge content and NCQD size, providing a predictive framework for tuning QD dimensions via compositional control of the starting $\text{Si}_{1-x}\text{Ge}_x\text{O}_2$ alloy.

The MD simulations successfully predict general trends in QD formation behaviour, which were corroborated by experimental STEM and XRD analysis. For the quantitative QD formation modelling, an analytical model was derived to predict the radius of Ge NCQDs and the surrounding oxide thickness as a function of the Ge content in $\text{Si}_{1-x}\text{Ge}_x\text{O}_2$ alloys. This model captures the redistribution of mass and volume during high-temperature annealing and provides a scalable framework for composition-driven NCQD design.

Assuming that the annealing time is enough so that most of the Ge atoms agglomerate, the mass and density relationships before and after annealing can be found. Besides, this

Table 2 Comparison of the MD simulation results with values calculated from Equation 3–5 for the size of Ge QDs after the annealing process. All samples were subsequently relaxed at 300 K.

x	Methods	α (t'/t)	R (nm)	d (nm)
0.10	Equation	0.976	1.04	1.19
	Simulation	0.947	0.68	0.49
0.17	Equation	0.960	1.56	1.23
	Simulation	0.938	1.33	1.39
0.20	Equation	0.951	1.17	0.79
	Simulation	0.888	0.88	0.95
0.25	Equation	0.940	1.79	0.96
	Simulation	0.889	1.60	1.00
0.30	Equation	0.928	1.88	0.82
	Simulation	0.887	1.75	0.83
0.35	Equation	0.916	2.01	0.70
	Simulation	0.870	1.70	0.88

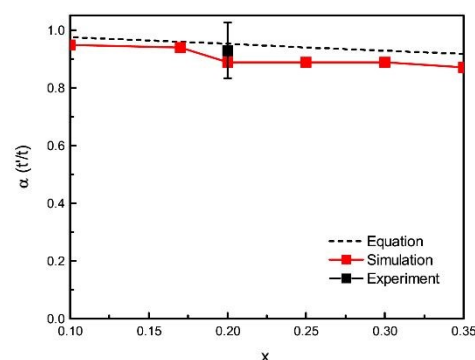


Fig. 7 Comparison of the oxide length ratio (α) obtained from simulations and experiments compared with the calculation from Equation 3–5. The x represents the Ge content relative to Si in the SiGeO alloy. For the experimental results, the error bar denotes the standard deviation (± 0.1).



assumption seems effective in most of the cases since we observed that 80–90% of the agglomeration was completed within 5–15 minutes of RTA. When the final NCQD radius is R and the tunnelling oxide thickness is d , which is equally distributed top and bottom of the NCQD, the initial volume of the SiGeO layer, $V_{initial}$, and the final volume, V_{final} , of Ge QD and the surrounding SiO₂ can be expressed in the following equations:

$$V_{initial} = \frac{N(1-x)m_{Si} + Nxm_{Ge} + 2Nm_O}{x\rho_{GeO_2} + (1-x)\rho_{SiO_2}} = t^3 \quad (2)$$

$$V_{final} = \frac{Nxm_{Ge}}{\rho_{Ge}} + \frac{N(1-x)m_{Si} + 2N(1-x)m_O}{\rho_{SiO_2}} = t'^3 \quad (3)$$

$$R = \left[\frac{3Nm_{Ge}x}{4\pi\rho_{Ge}} \right]^{1/3} \quad (4)$$

$$d = \frac{1}{2} \sqrt[3]{t' - t} \quad (5)$$

Here, t and t' represent the cube lengths of the oxide before and after annealing, which are derived from the density difference between the GeO_x and Ge QD. N is the total number of Si and Ge atoms, while x is the Ge content of Si_{1-x}Ge_xO₂ alloy. m and ρ are the atomic masses and material densities, respectively. Consequently, the tunnelling oxide thickness, d , can be determined using the final volume and the QD radius from the Equation 3 and 4, and expressed in Equation 5.

Model predictions were validated against MD simulations and the experimental results. The analytical model yielded results closely matching the MD data (Table 2). The slight discrepancy in QD radius (~0.25 nm) is attributed to the overestimation of Ge density in the MD simulation, likely due to the limited relaxation time following high-temperature annealing.

The oxide length ratio α , defined as t'/t , depends only on the Ge content, x , and remains independent of system size. This parameter captures the volumetric shrinkage resulting from the densification and crystallization of Ge within the oxide. As x increases, the difference in oxide lengths becomes more pronounced. In Fig. 7, the MD data yielded results closely matching the analytical model with the slightly underestimation in α , indicating that model predictions were validated against MD simulation for a 10–35% Ge alloy. For $x = 0.3$ in Fig. 6(h), the theoretical value of α was calculated to be 0.928, while the MD simulation yielded a slightly lower value of 0.887 due to the relatively small QD radius. When $x = 0.2$, the calculated ratio was 0.952 from the equations.

In experimental measurement in Fig. 7, the samples prepared by double-step annealing were closely fitted with the analytical model prediction. During oxidation, the Si_{0.5}Ge_{0.5} substrate forms a SiGeO alloy containing ~20% of Ge content. The Ge NCQD sample in Fig. 6 exhibits a slight overestimation of α (~0.045) and an underestimation of R (~0.13) as the Ge QDs were not fully crystallized and contained regions with GeO_x boundaries. Consequently, the ratio increased to 0.997.

Nevertheless, the enhanced Ge agglomeration achieved by double-step annealing ensures that the overall trend in both oxide length ratio and QD radius was consistent with the model's predictions.

The combination of MD simulations and experimental validation demonstrates that Ge NCQDs can be reliably synthesized within a SiO_x matrix from our method. The MD simulations provide valuable insights into the agglomeration dynamics of Ge atoms, predicting the QDs' sizes with different Ge contents. Experimental results corroborate these findings, showing that Ge NCQDs through the self-assembly method exhibit crystalline properties under optimized annealing conditions. Further, the analytical model provides a reliable first-order tool for predicting both the QD size and surrounding oxide thickness as functions of initial alloy composition and processing. This modelling approach enables rational design of Ge QD-based structures with tailored geometry for quantum confinement and efficient charge transfer. It serves as a valuable foundation for implementing predictive control in the quantum nanomaterial synthesis and device integration.

3 Conclusions

In this study, a deterministic and thermodynamically guided synthesis strategy was developed to form spatially confined Ge NCQDs within a silicon oxide matrix, enabling precise control over dot size and oxide thickness. By combining MD simulations, analytical modelling, and experimental validation, we demonstrated that the size and distribution of Ge QDs can be predictively tuned through the Ge content and thermal processing conditions, providing a CMOS-compatible pathway for engineering quantum-confined structures.

The double-step annealing process enabled the formation of spatially confined, single-row Ge NCQDs with a size of 9.2 nm, separated from the SiGe channel by oxide barriers as thin as 3.2 nm. Moreover, PL measurements confirmed size-dependent emission in the visible range, highlighting quantum confinement effects at room temperature. This work lays the foundation for materials-driven control of QD geometries, enabling a reproducible route toward next-generation QD technologies.

Author contributions

S. H. P.: conceptualization, methodology, investigation, software, data analysis, visualization, writing – original draft. G. M. S.: conceptualization, methodology, investigation, data analysis, visualization. J. W. K.: investigation, data analysis, visualization. Y. H. L.: investigation, data analysis, visualization. G. B. L.: methodology, visualization, investigation. H. J. L.: methodology, investigation. B. D. K.: conceptualization, methodology, supervision, resources, project administration, funding acquisition. All authors: writing – review & editing.



Conflicts of interest

There are no conflicts to declare

Data availability

Raw data are available from the corresponding author upon reasonable request.

Acknowledgements

This work was supported by 'Samsung Research Funding and Incubation Center' of Samsung Electronics (SRFC-IT2102-01) and the National Research Foundation (NRF) grant funded by the Korea government (Ministry of Science and ICT) (No. NRF-2021M3F3A2A03017770).

References

- D. S. Kumar, B. J. Kumar, and H. Mahesh, *Quantum nanostructures (QDs): an overview, in Synthesis of inorganic nanomaterials*, 2018, 59-88.
- L. E. Brus, Electron-electron and electron-hole interactions in small semiconductor crystallites: The size dependence of the lowest excited electronic state. *J. Chem. Phys.* 1984, **80**, 4403-4409.
- K. K. Likharev, Single-electron devices and their applications. *Proc. IEEE* 1999, **87**, 606-632.
- S. Krishnamurthy, *et al.*, PbS/CdS quantum dot room-temperature single-emitter spectroscopy reaches the telecom O and S bands via an engineered stability. *ACS nano* 2020, **15**, 575-587.
- W. Heiss, *et al.*, Highly luminescent nanocrystal quantum dots fabricated by lattice-type mismatched epitaxy. *Physica E Low Dimens. Syst. and Nanostruct.* 2006, **35**, 241-245.
- M. Aouassa *et al.*, Growth and characterization of SiGe/SiO₂ core/shell nanocrystals on insulators, *ACS Appl. Electron. Mater.* 2024, **6**, 4120-4129.
- M. Aouassa *et al.*, Growth of Ge QDs-decorated sige nanocrystals: toward integration of quantum dots and mie resonators in ultrathin film for photodetection and energy harvesting, *ACS Appl. Electron. Mater.* 2024, **6**, 3290-3296.
- M. A. Alenizi *et al.*, Electrical and dielectric characterization of Ge quantum dots embedded in MIS structure (AuPd/SiO₂: Ge QDs/n-Si) grown by MBE. *Physica B: Condens. Matter* 2024, **685**, 415962.
- T. C. Chen, L. S. Lee, W. Z. Lai, and C. W. Liu, The characteristic of HfO₂ on strained SiGe. *Mater. Sci. Semicond.* 2005, **8**, 209-213.
- E. Long, A. Galeckas, and A. Y. Kuznetsov, Ge concentrations in pile-up layers of sub-100-nm SiGe films for nano-structuring by thermal oxidation. *J. Vac. Sci. Technol. B* 2012, **30**, 041212.
- M. Kanoun, *et al.*, Electronic properties of Ge nanocrystals for non volatile memory applications. *Solid-State Electron.* 2006, **50**, 1310-1314.
- C. H. Kao, C. S. Lai, C. S. Huang, and K. M. Fan, Ge nanocrystal charge trapping devices fabricated by one-step oxidation on poly-SiGe. *Appl. Surf. Sci.* 2008, **255**, 2512-2516.
- W. K. Chim, Germanium Nanocrystal Non-Volatile Memory: Fabrication, Charge Storage Mechanism and Characterization. *Nanoscale* 2025, **14**, 4195.
- B. H. Koh, *et al.*, Traps in germanium nanocrystal memory and effect on charge retention: Modeling and experimental measurements. *J. Appl. Phys.* 2005, **97**, 124305.
- E. W. H. Kan, *et al.*, Effect of annealing profile on defect annihilation, crystallinity and size distribution of germanium nanodots in silicon oxide matrix. *Appl. Phys. Lett.* 2003, **83**, 2058-2060.
- W. R. Chen, T. C. Chang, Y. T. Hsieh, S. M. Sze, and C. Y. Chang, Formation of Ge nanocrystals using Si_{1.33}Ge_{0.67}O₂ and Si_{2.67}Ge_{1.33}N₂ film for nonvolatile memory application. *Appl. Phys. Lett.* 2007, **91**, 102106.
- M. Yang, *et al.*, Effect of annealing on charge transfer in Ge nanocrystal based nonvolatile memory structure. *J. Appl. Phys.* 2009, **106**, 103701.
- J. P. Zhao, *et al.*, Amorphous Ge quantum dots embedded in SiO₂ formed by low energy ion implantation. *J. Appl. Phys.* 2008, **103**, 124304.
- J. H. Wu and P. W. Li, Ge nanocrystals MOS capacitors with Ge nanocrystals formed by oxidation of poly-Si_{0.88}Ge_{0.12}. *Semicond. Sci. Technol.* 2006, **22**, S89-S92.
- C. H. Kao, C. S. Lai, M. C. Tsai, C. H. Lee, C. S. Huang, and C. R. Chen, Using thermal oxidation and rapid thermal annealing on polycrystalline-SiGe for Ge nanocrystals. *Mater. Res. Soc. Symp. Proc.* 2007, **1071**, 10710321.
- C. H. Kao, C. S. Lai, C. S. Huang, and K. M. Fan, Ge nanocrystal charge trapping devices fabricated by one-step oxidation on poly-SiGe. *Appl. Surf. Sci.* 2008, **255**, 2512-2516.
- A. Rodríguez, *et al.*, Ge nanocrystals embedded in a SiO₂ matrix obtained from SiGeO films deposited by LPCVD. *Semicond. Sci. Technol.* 2010, **25**, 045032.
- J. D. Cox, D. D. Wagman, and V. A. Medvedev, *CODATA key values for thermodynamics*, Hemisphere Publishing Corp., New York, 1989.
- D. C. Paine, C. Caragianis, and A. F. Schwartzman, Oxidation of Si_{1-x}Ge_x alloys at atmospheric and elevated pressure. *J. Appl. Phys.* 1991, **70**, 5076-5084.
- M. A. Nicolet and W. S. Liu, Oxidation of GeSi. *Microelectron. Eng.* 1995, **28**, 185-191.
- M. I. Richard, *et al.*, Tracking defect type and strain relaxation in patterned Ge/Si(001) islands by x-ray forbidden reflection analysis. *Phys. Rev. B* 2011, **84**, 075314.
- Q. Zheng, *et al.*, Unveiling the complexity of nanodiamond structures. *Proc. Natl. Acad. Sci. U. S. A.* 2023, **120**, e2301981120.
- Y. Maeda, Visible photoluminescence from nanocrystallite Ge embedded in a glassy SiO₂ matrix: evidence in support of the quantum-confinement mechanism. *Phys. Rev. B.* 1995, **51**, 1658-1670.
- Y. Maeda, N. Tsukamoto, Y. Yazawa, Y. Kanemitsu, and Y. Masumoto, Visible photoluminescence of Ge microcrystals embedded in SiO₂ glassy matrices. *Appl. Phys. Lett.* 1991, **59**, 3168-3170.
- K. Surana, P. K. Singh, H. W. Rhee, and B. Bhattacharya, Synthesis, characterization and application of CdSe quantum dots. *J. Ind. Eng. Chem.* 2014, **20**, 4188-4193.
- P. H. Liao, *et al.*, Size-tunable strain engineering in Ge nanocrystals embedded within SiO₂ and Si₃N₄. *Appl. Phys. Lett.* 2014, **105**, 172106.
- A. P. Thompson, *et al.*, LAMMPS-a flexible simulation tool for particle-based materials modeling at the atomic, meso, and continuum scales. *Comput. Phys. Commun.* 2022, **271**, 108171.
- J. K. Bording, Molecular-dynamics simulation of Ge rapidly cooled from the molten state into the amorphous state. *Phys. Rev. B* 2000, **62**, 7103-7109.



Data Availability

The data that support the findings of this study are available in the supporting material and available from the corresponding author upon reasonable request.

